J Solid State Electrochem (2007) 11:1593–1603
DOI 10.1007/s10008-006-0198-8

ORIGINAL PAPER

Electrodeposition of lead on glassy carbon and mercury film electrodes from a distillable room temperature ionic liquid, DIMCARB

Anand I. Bhatt · Alan M. Bond · Jie Zhang

Received: 2 May 2006 / Revised: 22 May 2006 / Accepted: 31 May 2006 / Published online: 12 September 2006

Abstract The electrochemical reduction of Pb^{2+} has been studied in the 'distillable' ionic liquid DIMCARB (a mixture of adducts of dimethylamine and carbon dioxide, comprising both neutral and ionic moieties). Voltammetric results show that Pb^{2+} is reduced in a single step to form Pb metal via a nucleation and growth mechanism on a glassy carbon electrode. Ex situ powder X-ray diffraction studies on deposited lead show the presence of both α- and β-PbO_2, as well as elemental lead, suggesting the finely deposited lead particles are in an active rather than passive state. Chronamperometric and scanning electron microscope measurements show that the nucleation and growth follows a progressive nucleation mechanism on glassy carbon. Large peak–peak separations for the Pb reduction and oxidation are consistent with this mechanism and do not suggest electrochemical reversibility. However, experiments with co-deposition of Hg show that this irreversibility is a result of deposition onto a solid glassy carbon surface rather than a solvent effect. The diffusion coefficient of Pb^{2+} in DIMCARB has been calculated to be $1.8\pm0.4\times10^{-7}$ cm^2 s^{-1}.

Keywords Lead · DIMCARB · Voltammetry · Dialcarbs · Distillable room temperature ionic liquids · Glassy carbon · Nucleation and growth

Introduction

Considerable research on the electrochemical use of room temperature ionic liquids (RTIL) or low-temperature ionic liquids is presently being undertaken because of their advantageous properties of high conductivity and significant electrochemical stability, which can be selectively controlled by changing the cation or anion [1–7]. The abilities to dissolve a wide range of organic and inorganic compounds and to act as the electrolyte are also attractive features [1–7]. However, there are problems when the separation of ionic liquids from electrosynthesised products is required and also in the recovery of ionic liquids for further use or disposal. This is because commonly used ionic liquids, unlike organic solvents, do not posses any significant vapour pressure, and hence, conventional solvent distillation techniques cannot be used readily to achieve these outcomes.

One solution to ionic liquid recovery is to use 'distillable' ionic liquids, such as those based on *N*,*N*-dialkylammonium *N*′,*N*′-dialkylcarbamate melts (dialcarbs) [8, 9], which are, in fact, easily recovered by distillation techniques. Dialcarbs are mixtures of CO_2 and dialkylamines (general formula R′RNH, where R and R′=alkyl group), which upon mixing at low temperatures form ionic melts. In addition, dialcarbs also have advantages

Electronic supplementary material Supplementary material is available in the online version of this article at http://dx.doi.org/10.1007/s10008-006-0198-8 and is accessible for authorized users.

This work is dedicated to Piero Zanello on the occasion of his 65th birthday in recognition of his numerous contributions to inorganic electrochemistry.

A. I. Bhatt · A. M. Bond · J. Zhang
School of Chemistry, Monash University,
Clayton, Victoria 3800, Australia

A. I. Bhatt · A. M. Bond (✉)
ARC Special Research Centre for Green Chemistry,
Monash University,
Clayton, Victoria 3800, Australia
e-mail: alan.bond@sci.monash.edu.au

associated with a low cost of synthesis and high, tuneable conductivities achieved by varying the CO_2:R′RNH ratio.

The stoichiometric compound *N*,*N*-dimethylammonium *N*′,*N*′-dimethylcarbamate ($[Me_2NH_2]^+[Me_2N—CO_2]^-$) has a melting point around 35 °C [8, 9]. However, by limiting the amount of Me_2NH, a liquid DIMCARB comprising an Me_2NH and CO_2 ratio of 1.8:1 can be formed, which achieves the desirable outcome of being a liquid at room temperature [8–10].

In a recent brief survey of the use of DIMCARB as an electrochemical solvent, it was demonstrated that this distillable RTIL medium should be ideal for metal deposition reactions because of the wide negative potential range available [10]. In this paper we provided mechanistic details of the $Pb^{2+} + 2e^- \rightarrow Pb_{(metal)}$ and $Pb^{2+} + 2e^- \xrightarrow{Hg} Pb_{(amalgum)}$ reduction processes in DIMCARB and use this model system to gain an insight into the use of this 'distillable' ionic liquid as a medium for metal deposition. In particular, it has been noted that mechanisms for metal deposition processes can be very solvent-dependent. Little is known about the deposition of lead from ionic liquids [11]. Thus, results in DIMCARB are compared to those reported for deposition in water to ascertain if any differences are detected in this media [12].

Materials and methods

Reagents and chemicals

$Pb(CO_2CH_3)_2.3H_2O$ (BDH), $Pb(NO_3)_2$ (Aldrich), $Pb(CO_3)_2$ (Aldrich), decamethylferrocene (DmFc) (Aldrich), cobaltocinium hexafluorophosphate (Strem), $Hg(CO_2CH_3)_2$ (Hopkin and Williams) and lead metal (Aldrich, 99.99%) were purchased from commercial sources and used as supplied. DIMCARB was prepared as previously reported [10]. Briefly, solid CO_2 and dimethylamine gases were combined at a slow rate for ca. 4 h until clear colourless liquid DIMCARB was obtained.

Electrochemical instrumentation and techniques

Voltammetric and chronoamperometric studies were undertaken with a VoltaLab PGZ301 potentiostat (Radiometer Analytical) operated by VoltaLab Software (version 4). Rotating disk electrode (RDE) voltammograms were obtained by combining the VoltaLab system with a Metrohm 628-10 RDE assembly. All data were obtained in a conventional three-electrode cell using a glassy carbon working electrode (0.0707 cm^2) and a Pt counter electrode. The reference electrode consisted of a silver wire quasi reference electrode (QRE) immersed into DIMCARB and separated from the bulk solution with a glass frit. For RDE studies, a glassy carbon electrode (0.0707 cm^2) and the aforementioned counter and reference electrodes were used. Oxygen dissolved in DIMCARB was removed by degassing with nitrogen or carbon dioxide. Unless otherwise stated, all potentials reported in this paper are quoted vs $DmFc^+$/DmFc couple or the Ag wire QRE, which has a potential of −0.24 V vs $DmFc^{+/0}$.

Microelectrode data were obtained using a carbon fibre sealed in a glass tube with the aforementioned counter and reference electrodes. Prior to measurements, the electrode radius was calculated by measuring steady state cyclic voltammograms for the $[Fe(CN)_6]^{4-/3-}$ couple using $K_4[Fe(CN)_6].3H_2O$ (4.97 mM) in 0.1 M KCl with a saturated calomel electrode reference electrode and a Pt counter electrode (assuming a D value of 0.65×10^{-5} cm^2 s^{-1} [13]).

Bulk reductive electrolysis of Pb(II) was achieved by placing 10 mL of Pb/DIMCARB solution into a cell equipped with a 0.5-cm-diameter glassy carbon rod working electrode, Pt gauze counter electrode and the Ag wire QRE. This solution was separated from the Pt gauze counter electrode using a glass frit. Powder X-ray diffraction examination of the product was obtained with a Phillips 1729 diffractometer (Cu-α radiation source) and analysed with the assistance of Traces software. Samples of electrochemically deposited lead were washed twice with acetone and allowed to air dry for 3 days prior to analysis. Images of lead deposits on GC electrodes were obtained with a Jeol JSM-840A scanning electron microscope (SEM) fitted with an Oxford Link energy-dispersive X-ray (EDAX) system. Samples were prepared by placing a freshly polished glassy carbon working electrode into a 5-mM solution of $Pb(CO_2CH_3)_2.3H_2O$ in DIMCARB and initially holding the electrode potential at 0.0 V vs Ag wire QRE for 30 s to electrochemically clean the electrode surface. The potential was then held at −0.75 V for 20 s to deposit Pb onto the electrode surface. Finally, the electrode was removed from solution and cleaned with acetone prior to SEM examination.

Results and discussion

Pb deposition from DIMCARB at a glassy carbon working electrode

Hydrodynamic voltammetry

Voltammograms obtained for reduction of Pb^{2+} in DIMCARB at a glassy carbon RDE are shown in Fig. 1. For all Pb(II) compounds investigated, at both 1 and 5 mM concentrations, the voltammograms exhibit one reduction and one oxidation component. The reduction process has a

steady-state sigmoidal shape and is assigned to the Pb^{2+}/Pb^{0} reduction process, whilst the peak shape associated with the oxidation process is attributable to the Pb^{0}/Pb^{2+} stripping reaction. At the initial potential, until about −0.95 V vs $DmFc^{+}$/DmFc, voltammograms exhibit essentially zero current. In the potential range of −0.95 to −1.05 V vs $DmFc^{+}$/DmFc, the current rises until an almost constant value is reached and maintained until the switching potential of −1.5 V vs $DmFc^{+}$/DmFc. After switching the potential direction, a very small increase in the limiting current value is detected, until a sharp stripping peak with a maximum current at E_p^{ox}, after which the current rapidly decays back to zero. All these data are consistent with Pb being deposited on the GC RDE when the potential is sufficiently negative and then being stripped off from the surface at sufficiently positive potentials. That is, the reduction component is described by Eq. 1 and the oxidation component by Eq. 2:

$$Pb^{2+}_{(soln)} + 2e^{-} \rightarrow Pb_{(metal)} \quad (1)$$

$$Pb_{(metal)} \rightarrow Pb^{2+}_{(soln)} + 2e^{-} \quad (2)$$

Voltammetry at a glassy carbon microelectrode

Voltammograms of Pb(II) reduction in a stationary solution were recorded at a glassy carbon microelectrode at four different concentrations (ca. 5, 10, 20 and 25 mM) and also exhibit one reduction and one oxidation component. As is the case at the RDE, the reduction portion is sigmoidal shaped and rises to a steady-state limiting current (I_{ss}), whilst the oxidation component exhibits a peak current at E_p^{ox} and then rapidly decays to zero.

Cyclic voltammetry

Cyclic voltammograms obtained over the concentration range of 1–5 mM when $Pb(CO_2CH_3)_2.3H_2O$, $Pb(NO_3)_2$ and $Pb(CO_3)_2$ are dissolved in DIMCARB were recorded at a glassy carbon working electrode as a function of scan rate. Figure 2 provides typical responses under a range of conditions. Data related to peak potentials obtained at about 5 mM concentration are summarised in Table 1 with data for the 1-mM solutions given in the Electronic supplementary material. Under all conditions examined, cyclic voltammograms exhibit a broad reduction peak and a much sharper, more symmetrical oxidation peak, which is typical of metal plating stripping behaviour. The reduction and oxidation processes give rise to large peak–peak separations. However, the midpoint potentials (E_m) all lie in the range of −900 to −1,100 mV vs $DmFc^{+}$/DmFc under the conditions of Table 1. In general, potentials are not strongly dependant on the source of Pb(II), but a small concentration dependence is evident (Table 1). The scan rate dependence is interesting in that the oxidation or stripping peak potential shifts by less than 50 mV over the scan rate range of 2–200 mV s^{-1}, whereas much larger reduction peak shifts of around 300 mV are detected over the same range. These data

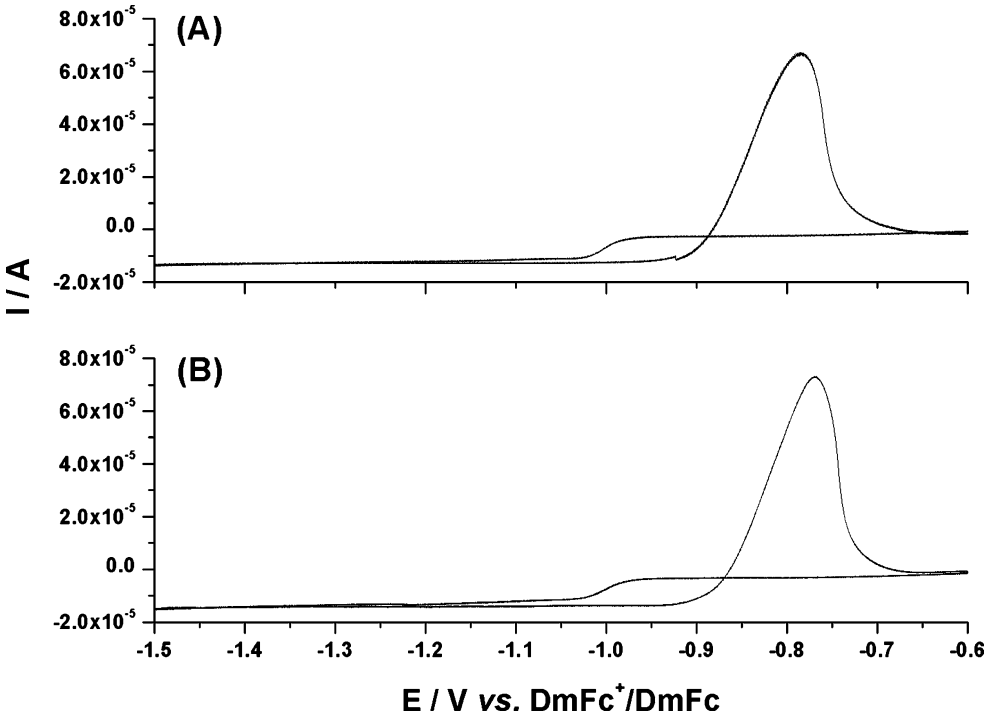

Fig. 1 Rotating glassy carbon disk electrode voltammograms obtained for reduction of Pb(II) in DIMCARB at 25 °C. Rotation rate=500 rpm, scan rate=0.005 V s^{-1}; **a** 4.8 mM $Pb(NO_3)_2$; **b** 4.9 mM $Pb(CO_3)_2$

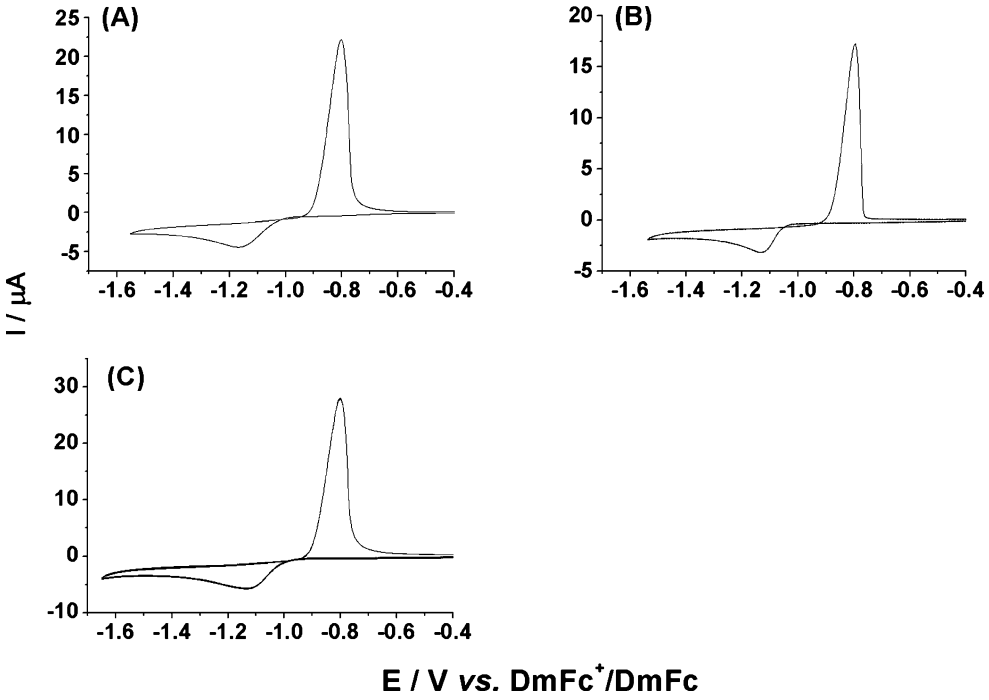

Fig. 2 Cyclic voltammograms obtained at 25 °C for reduction of Pb(II) in DIMCARB at a glassy carbon electrode. Scan rate=0.1 V s^{-1}; **a** 4.8 mM $Pb(NO_3)_2$; **b** 4.9 mM $Pb(CO_3)_2$; **c** 4.9 mM $Pb(CH_3COO)_2.3H_2O$

are consistent with a nucleation and growth process for plating of lead onto a GC electrode in the reduction step and subsequent stripping of $Pb_{(metal)}$ in the oxidation component.

As expected for a nucleation–growth-type deposition step, the nature of the cyclic voltammograms is a function of switching potential (Fig. 3) [13]. Thus, when the potential is switched at potentials slightly more negative than E_p^{red}, a well-defined crossover current is detected shortly after reversing the scan direction. As found in aqueous media, this behaviour is consistent with a 3-D nucleation and growth mechanism for Pb deposition on glassy carbon in DIMCARB rather than the formation of a thin film of lead [14, 15]. No evidence for Pb under-potential deposition was detected.

Chronoamperometric study of Pb deposition from DIMCARB: glassy carbon working electrode

Chronoamperometry is an informative technique for probing the mechanism of a deposition reaction [16–18]. In the chronoamperometric experiments for the reduction of Pb(II) in DIMCARB, the initial potential was set at a value that was much less negative than required for the reduction of Pb(II) and then stepped to potentials where reduction occurs. Current–time responses obtained for Pb^{2+} reduction in DIMCARB as a function of stepping potential are presented in Fig. 4. Initially, a large capacitance current is detected, which decays rapidly. At longer times, the time dependence of Faradaic current can be readily detected. The Faradaic current transients obtained at the longer times

Table 1 Cyclic voltammetry parameters for solutions of $Pb(NO_3)_2$ (5.1 mM), $Pb(CO_3)_2$ (4.8 mM) and $Pb(CO_2CH_3)_2.3H_2O$ (4.6 mM) in DIMCARB. All potentials referenced to $DmFc^+$/DmFc

Scan rate/ mV s^{-1}	$Pb(CO_2CH_3)_2.3H_2O$					$Pb(CO_3)_2$					$Pb(NO_3)_2$				
	E_p^{red}/ mV	E_p^{ox}/ mV	ΔE_p/ mV	E_m/ mV	$w_{1/2}$/ mV	E_p^{red}/ mV	E_p^{ox}/ mV	ΔE_p/ mV	E_m/ mV	$w_{1/2}$/ mV	E_p^{red}/ mV	E_p^{ox}/ mV	ΔE_p/ mV	E_m/ mV	$w_{1/2}$/ mV
2	−1,015	−850	165	−933	33	−1,016	−853	163	−935	33	−1,005	−844	161	−925	34
5	−1,047	−840	207	−944	40	−1,044	−849	195	−947	41	−1,040	−839	201	−940	43
20	−1,075	−820	255	−948	55	−1,092	−836	256	−964	53	−1,092	−827	265	−960	56
40	−1,132	−814	318	−973	61	−1,131	−848	283	−990	70	−1,161	−815	346	−988	64
60	−1,152	−806	346	−979	72	−1,154	−806	348	−980	78	−1,196	−811	385	−1,004	70
80	−1,198	−802	396	−1,000	72	−1,176	−801	375	−989	80	−1,234	−808	426	−1,021	72
100	−1,221	−801	420	−1,011	72	−1,175	−797	378	−986	85	−1,269	−804	465	−1,037	74
200	−1,332	−792	540	−1,062	77	−1,278	−800	478	−1,039	85	−1,344	−785	559	−1,065	86

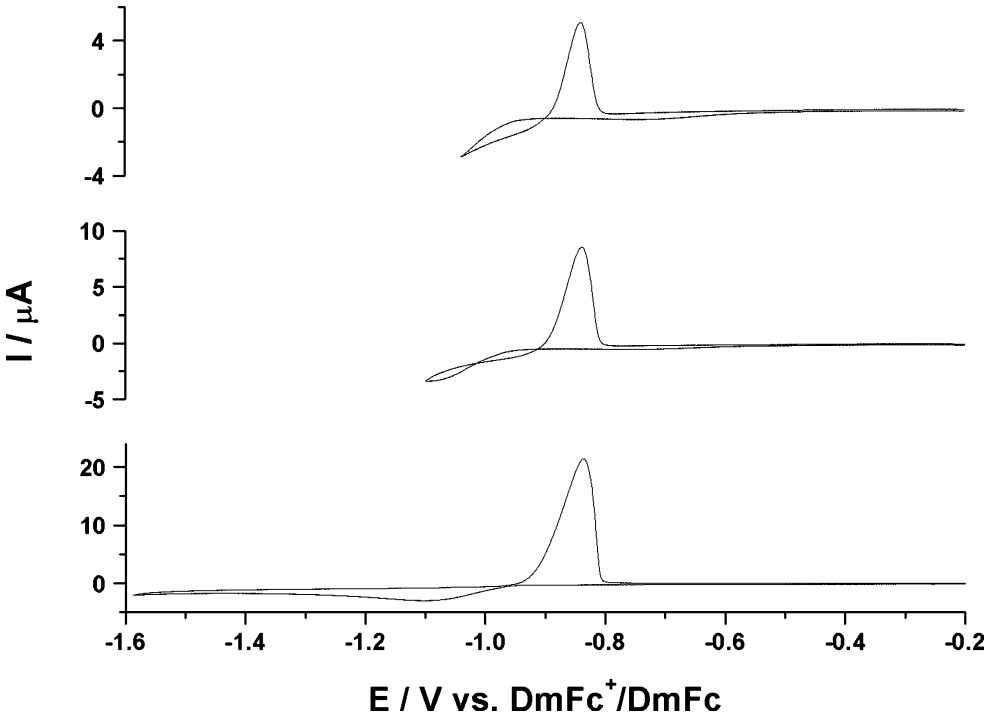

Fig. 3 Cyclic voltammograms obtained for reduction of 4.8 mM $Pb(NO_3)_2$ as a function of switching potential, scan rate=0.04 V s^{-1}, T=25 °C

show that when the potential is stepped to values that are close to E_p^{red}, a maximum current value (I_m) is quickly achieved, which then at longer times decays to a diffusion-limited steady state current. When the potential is stepped to a value that is very negative relative to E_p^{red}, then the well-known $t^{-1/2}$ (t=time) Cottrellian decay [13] is detected and no current maximum is observed. This time and potential stepping behaviour is consistent with that expected for the deposition of lead onto an electrode surface via a nucleation and growth phenomenon [16–21], as is also suggested by the voltammetric studies.

The initial stages of electrochemical deposition are usually associated with either a 2-D or a 3-D nucleation and growth process [19–21]. Models have been developed to predict the current transients obtained for different mechanisms. For metal deposition, 3-D nucleation with diffusion-controlled growth represents a commonly reported model [17–19]. However, the nucleation mechanisms may be of two different types [19–21]. In one case,

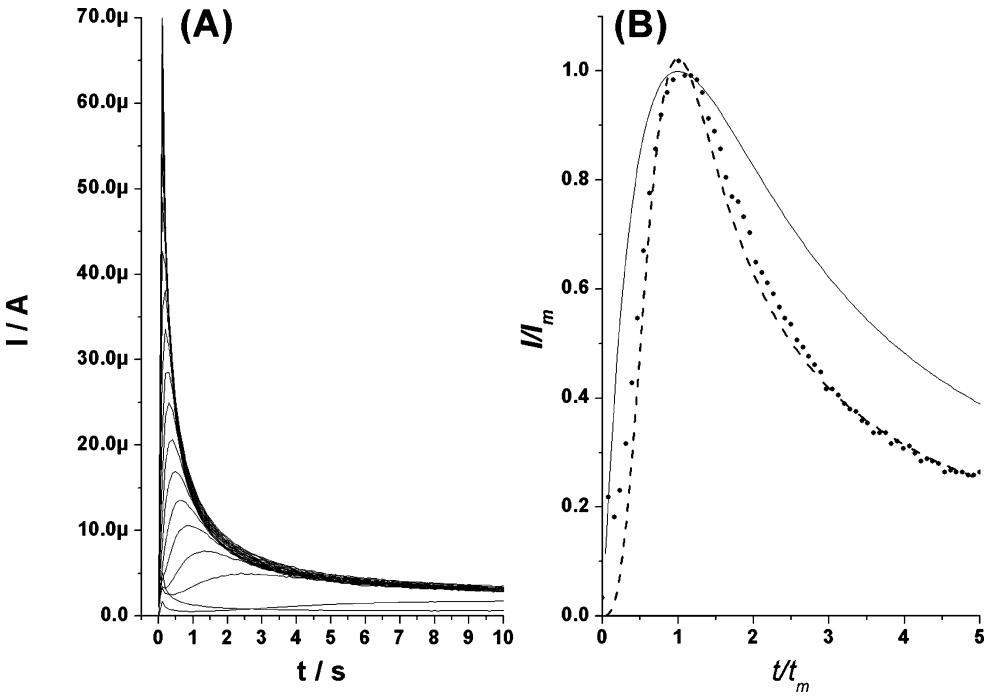

Fig. 4 **a** Chronoamperometric current vs time responses obtained for reduction of 4.9 mM $Pb(NO_3)_2$ in DIMCARB at 25 °C when the potential is stepped from an initial value where no reduction occurs to progressively more negative potentials where the Pb(II)+$2e^-$→Pb process occurs (0.0 V to −1.2 V with 40 mV increments). **b** Comparison of experimental plot of I/I_m vs t/t_m obtained from chronoamperometric experiments for reduction of 4.9 mM $Pb(NO_3)_2$ in DIMCARB at 22 °C when the potential was stepped from 0.0 to −0.66 V (*dotted line*) and theoretical plots derived from the instantaneous nucleation [Eq. 2 (*solid line*)] and progressive nucleation [Eq. 3 (*broken line*)] models

instantaneous nucleation occurs in which adatoms of metal are deposited on the electrode surface and uniformly cover the entire surface. These adatoms then all grow in size at a constant rate that is dependent on the potential [19–21]. In an alternative mechanism, progressive rather than uniform growth occurs, which assumes that as adatoms of metal are deposited, they grow at differing rates which depend on the time of their deposition [19–21].

The current transients for lead deposition from DIMCARB have been analysed using the methodology developed by Hills and Scharifker [21]. These authors showed that the two types of nucleation mechanism may be distinguished by the comparison of experimental data with normalised growth laws that can be predicted in terms of the ratio of current, I, obtained at time t to the maximum current obtained (I_m) at time t_m. In the case of instantaneous growth [21]:

$$\left(\frac{I}{I_m}\right)^2 = \frac{1.9542}{(t/t_m)}\left\{1 - exp\left[-1.2564\left(\frac{t}{t_m}\right)\right]\right\}^2 \quad (3)$$

In contrast, for a progressive nucleation mechanism [21],

$$\left(\frac{I}{I_m}\right)^2 = \frac{1.2254}{(t/t_m)}\left\{1 - exp\left[-2.3367\left(\frac{t}{t_m}\right)^2\right]\right\}^2 \quad (4)$$

Plots of $(I/I_m)^2$ vs t/t_m for Pb(II) reduction in DIMCARB compared with the theoretical predictions based on Eqs. 3 and 4 are shown in Fig. 4 for one set of experiments. In all cases, the use of Eq. 4 provides a far better fit of the experimental data, thereby suggesting that lead deposition onto a glassy carbon electrode from DIMCARB occurs predominantly via a progressive nucleation mechanism. This mechanism was also found for the deposition onto a glassy carbon electrode of Pb from emimCl/$AlCl_3$ [22] and for lead from aqueous media [14, 15].

Controlled potential electrolysis and scanning electron microscopy

To confirm that elemental lead is deposited on the GC surface, controlled potential electrolysis experiments were undertaken at potentials more negative than E_p^{red}. A grey deposit was detected upon the completion of electrolysis via visual inspection of the electrode surface after its removal from DIMCARB. X-ray diffraction analysis of the product showed evidence of the expected metallic Pb, as well as α- and β-PbO_2 phases (Fig. 5) [23–25]. A sample of pure lead metal was treated under the same sample preparation conditions as for the electrochemically deposited lead. The X-ray diffraction analysis of this sample showed only peaks attributed to Pb metal. The presence of the lead oxide phases observed in the electrochemically deposited lead implies that highly activated rather than passivated microparticles of lead are formed, which rapidly react with oxygen.

Examination of the glassy carbon electrode surface after bulk electrolysis by the SEM method revealed (Fig. 6) that a very non-uniform range of Pb deposition

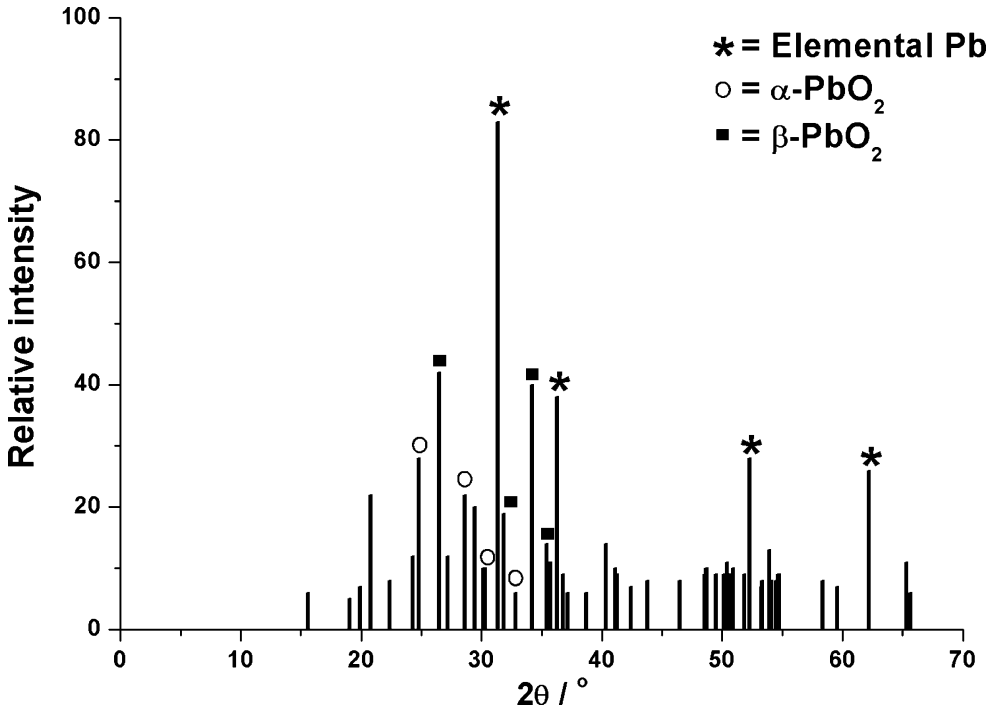

Fig. 5 Ex situ X-ray powder diffraction patterns obtained after Pb is electrodeposited from DIMCARB using bulk electrolysis at a glassy carbon rod working electrode. *Asterisk* denotes 2θ values attributable to elemental Pb [11], *circle* denotes 2θ values attributable to α-PbO_2 [11] and *square* denotes 2θ values attributable to β-PbO_2 [11]

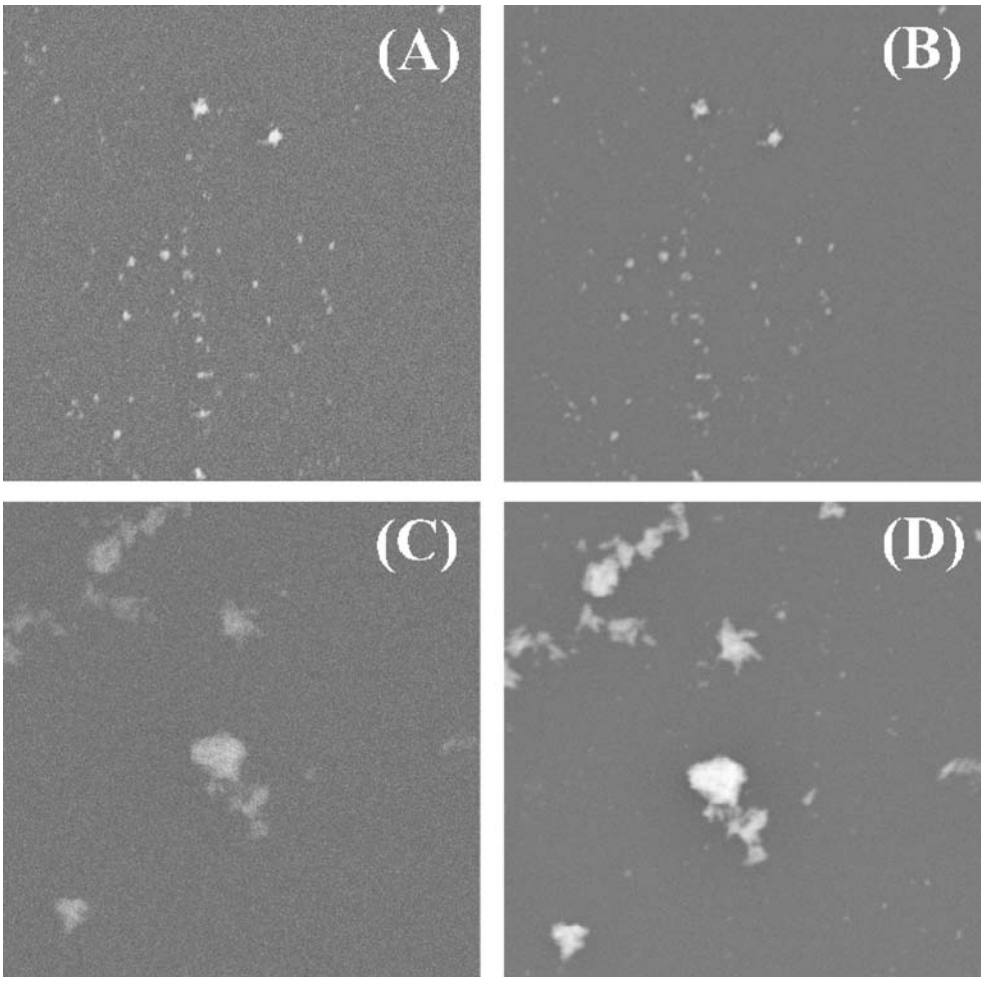

Fig. 6 Ex situ SEM images obtained after Pb is deposited from DIMCARB onto a glassy carbon electrode; **a** secondary electron image at 1,000× magnification; **b** elemental Pb composition map at 1,000× magnification; **c** secondary electron image at 5,000× magnification; **d** elemental Pb composition map at 5,000× magnification

sites (confirmed using EDAX) had formed rather than a thin film. This result supports the hypothesis that the deposition mechanism follows a nucleation and growth mechanism. If an instantaneous nucleation mechanism were operative, then the Pb deposition would consist of a uniform coverage of similar-sized nuclei. However, the SEM image provides evidence for a wide range of deposited lead sizes, which supports the progressive growth mechanism suggested on the basis of the analysis of data obtained by chronoamperometric experiments.

Pb deposition from DIMCARB at a mercury film electrode

Mercury deposition

Cyclic voltammograms of 8.5 mM $Hg(CO_2CH_3)_2$ in DIMCARB were recorded at a glassy carbon working electrode as a function of scan rate. Figure 7 provides typical responses observed under a range of conditions with relevant data summarised in Table 2. Under all conditions, the cyclic voltammograms exhibit a broad reduction peak, and a much sharper, more symmetrical oxidation peak typical of metal stripping components. As was previously observed for the Pb^{2+}/Pb^{0} process in DIMCARB, the reduction and oxidation components are well separated. The midpoint potentials lie in the range of −290 to −350 mV vs $DmFc^{+}$/DmFc. Also, as was previously observed for the reduction of Pb^{2+} to Pb in DIMCARB, the voltammetric waveshapes are strongly dependant on the switching potential. Switching at values slightly more negative than E_p^{red} results in a crossover of the cathodic and anodic currents indicative of a nucleation–growth process (in this case, droplets of Hg at the electrode surface) [26, 27]. However, at potentials much more negative than E_p^{red}, this effect is not observed.

Pb deposition on a mercury film

As the Hg reduction potential is well removed from that of the Pb(II), a mercury film electrode may thus be prepared in situ by the inclusion of Hg(II) into a DIMCARB solution

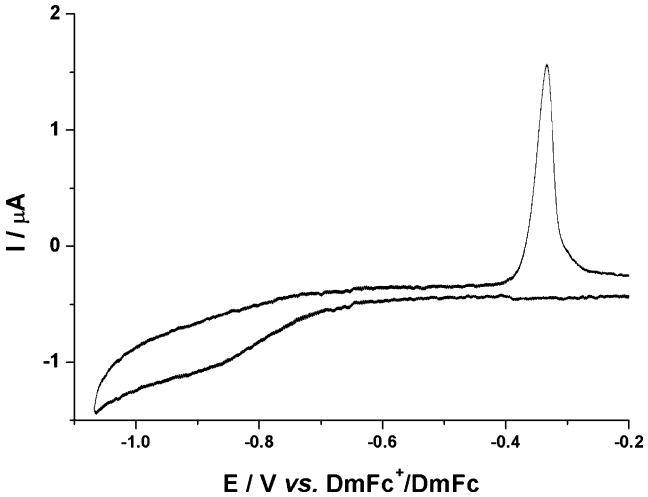

Fig. 7 Cyclic voltammograms obtained at a scan rate of 10 mV s^{-1} for reduction of 8.5 mM $Hg(CH_3COO)_2$ in DIMCARB at 22 °C

containing Pb(II). The Pb(II) reduction mechanism at a mercury film electrode can occur according to the following equation:

$$Pb^{2+} + 2e^- \xrightarrow{Hg} Pb_{(amalgum)} \quad (5)$$

Cyclic voltammograms of a solution containing both Hg^{2+} and Pb^{2+} are shown in Fig. 8. Voltammetric potential parameters obtained as a function of scan rate are summarised in Table 2. The reduction and oxidation processes in Fig. 8a at ca. −0.70 (designated as process I in Fig. 8a) and 0.40 V (designated as process II) are due to Hg deposition onto a GC electrode whilst the waves at ca. −1.20 (process III) and −1.10 V (process IV) are due to Pb plating to form an amalgam and stripping, respectively. Because the Hg(II) reduction occurs prior to that of Pb(II), the in situ formation of a Hg film electrode is achieved. In the case of the Pb(II)/Pb(0) processes, significant differences in the voltammograms are observed relative to those obtained at a glassy carbon electrode. The peak-to-peak separations at the mercury film electrode, whilst still dependent on scan rate, are much smaller than those found at a bare glassy carbon electrode. Cyclic voltammetric experiments at the mercury film electrode provide no evidence for current crossover when the potential is switched just past the peak potential (Fig. 8b) because amalgam formation does not require nucleation and growth of Pb metal particles.

Diffusion coefficient of Pb(II) in DIMCARB

The calculation of diffusion coefficients can be complicated if the depositing species is conducting (as is the case for metal deposition) because the effective electrode area changes during the course of the experiment. As a result, the diffusion coefficient of Pb(II) in DIMCARB has been calculated using a range of methods. Recently, Compton and Hyde have reported on the theory of metal deposition under hydrodynamic conditions. Their theory allows the diffusion coefficient (D) to be estimated using Eq. 6 [28] and has the advantage that the electrode area need not be known to calculate this parameter.

$$J_{LIM} = nFC_{BULK}\frac{D}{\delta} \quad (6)$$

where J_{LIM} is the current density, δ is the diffusion layer thickness, C_{BULK} is the bulk concentration, n=2 for lead deposition and other symbols have their usual meaning. δ values were calculated over the range of 500–3,000 rpm from Eq. 6 using the limiting current value obtained from the reduction of 5.1 mM cobaltocinium cation (Cc^+) in DIMCARB and assuming a D value of 1.2×10^{-7} cm^2 s^{-1} for Cc^+ [10, 28]. The average value of D calculated for

Table 2 Cyclic voltammetry parameters for solutions of 8.5 mM $Hg(CO_2CH_3)_2$ in DIMCARB and a solution of 5.4 mM $Pb(CO_2CH_3)_2.3H_2O$ with 5.0 mM $Hg(CO_2CH_3)_2$ at 22 °C. All potentials referenced to $DmFc^+$/DmFc

Scan rate/ mV s^{-1}	$Hg(CO_2CH_3)_2$				$Hg(CO_2CH_3)_2$ and $Pb(CO_2CH_3)_2.3H_2O$							
					$Pb(CO_2CH_3)_2.3H_2O$				$Hg(CO_2CH_3)_2$			
	E_p^{red}/ mV	E_p^{ox}/ mV	ΔE_p/ mV	E_m/ mV	E_p^{red}/ mV	E_p^{ox}/ mV	ΔE_p/ mV	E_m/ mV	E_p^{red}/ mV	E_p^{ox}/ mV	ΔE_p/ mV	E_m/ mV
1	−508	−72	436	−290	−895	−829	66	−862	−439	−72	367	−256
2	−531	−73	458	−322	−901	−829	72	−865	−448	−72	376	−260
5	−583	−72	511	−328	−926	−834	92	−880	−491	−72	419	−282
10	−596	−70	526	−333	−951	−842	109	−897	−548	−72	476	−310
20	−604	−71	533	−338	−952	−831	121	−892	−448	−72	376	−260
40	−640	−72	568	−356	−1,006	−859	147	−833	−618	−72	546	−345

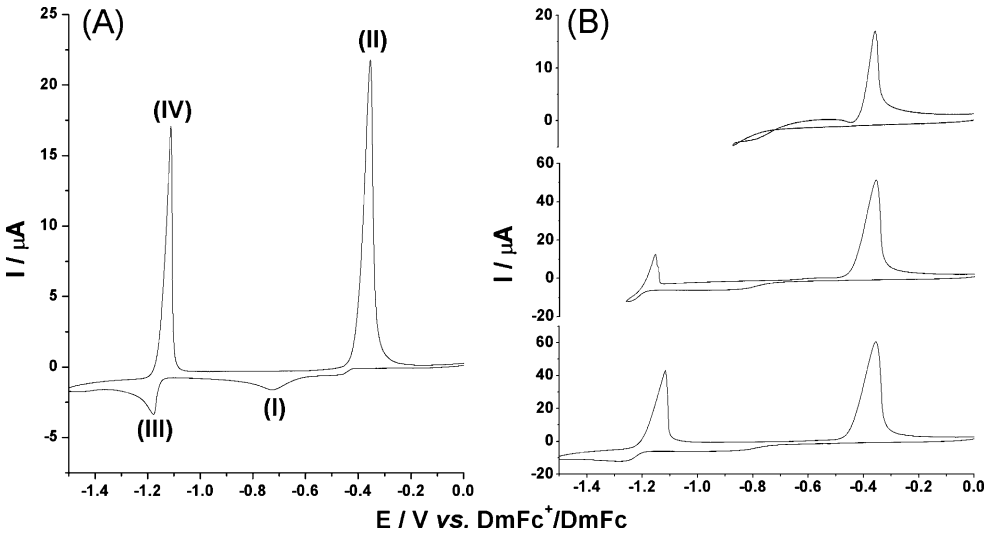

Fig. 8 **a** Cyclic voltammograms obtained at a scan rate of 1 mV s^{-1} in DIMCARB for reduction of 5.0 mM $Pb(CH_3COO)_2.3H_2O$ and 5.4 mM $Hg(CH_3COO)_2$ at 22 °C. **b** Effect of switching potential at a scan rate of 40 mV s^{-1}

Pb(II) in DIMCARB using this method was found to be $1.8\pm0.3\times10^{-7}$ cm^2 s^{-1}.

The diffusion coefficient of Pb(II) in DIMCARB also can be calculated from the thin-film electrode data using the theory developed by de Vries and van Dalen [29, 30]. For a reversible formation of a metal alloy (as approximately observed for Pb on Hg in DIMCARB), the following equations describe the deposition process:

$$I_p = 1.1157 \times 10^8 n^2 A C_{BULK} \nu L \tag{7}$$

$$n(E_p - E_{1/2}) = -1.43 + 29.58 \log H \tag{8}$$

$$H = \frac{L^2(nF\nu/RT)}{D} \tag{9}$$

where L is the Hg film thickness, H is a dimensionless parameter, A is the electrode area, ν is the scan rate and other symbols are defined elsewhere or have their usual meaning.

Using Eqs. 7, 8 and 9 and the data obtained for a solution of 5 mM lead acetate and mercury acetate in DIMCARB at 1 mV s^{-1}, the diffusion coefficient was calculated to be $1.8\pm0.4\times10^{-7}$ cm^2 s^{-1} and is in excellent agreement with that obtained from the theory of Compton and Hyde. Based on the consideration of results from the Compton–Hyde and de Vries–van Dalen theories, a reliable D value for Pb(II) in DIMCARB is believed to be $1.8\pm0.4\times10^{-7}$ cm^2 s^{-1}.

The theory of Hills and Scharifker is also commonly used to predict the diffusion coefficient when a deposition reaction proceeds via a nucleation–growth mechanism. This theory states that the diffusion coefficient, D, is linearly related to the product $I_m^2 t_m$ (where I_m and t_m are obtained from chronoamperometric data) [21]. For a progressive growth mechanism (as is the case for Pb in DIMCARB), D can be calculated using the following relationship:

$$I_m^2 tm = 0.2598(nFAC_{BULK})^2 D \tag{10}$$

Diffusion coefficients calculated using Eq. 10 predict values in the range of $0.9–2.0\times10^{-7}$ cm^2 s^{-1} but exhibit a systematic variation (the average value is 1.4×10^{-7} cm^2 s^{-1}, see Electronic supplementary material for further details). However, the product $I_m^2 t_m$ should be independent of the stepping potential, but for this system, this is not the case. Uncompensated resistance effects distort chronoamperometric data and may give rise to these discrepancies in the moderately resistive DIMCARB. Nevertheless, the values calculated are still close to those predicted by the Compton–Hyde and de Vries–van Dalen theories.

To a first approximation, D values can be calculated from the Cottrellian decay slopes if the effect of the growth of the electrode area is neglected due to Pb metal deposition. D values calculated from the Cottrell equation [13] gave a value of 3.0×10^{-7} cm^2 s^{-1}. Similarly, D values calculated at a GC RDE using the Levich equation [13] and at a GC microelectrode gave D values significantly higher than the value of 1.8×10^{-7} cm^2 s^{-1} calculated using the Compton–Hyde, de Vries–van Dalen and Hills–Scharifker approaches. The non-ideality is clearly demonstrated by a distinctly non-linear plot of I_p vs Pb^{2+} concentration detected at a GC RDE with a fixed rotation rate (Fig. 9). A linear dependence is predicted from the Levich equation assuming the electrode area does not change because of Pb deposition (it is possible that the addition of high concentrations of Pb^{2+} to DIMCARB alters the kinematic viscosity). Consequently, the values calculated using steady state methods may tend to over-predict the D value for Pb(II) in DIMCARB.

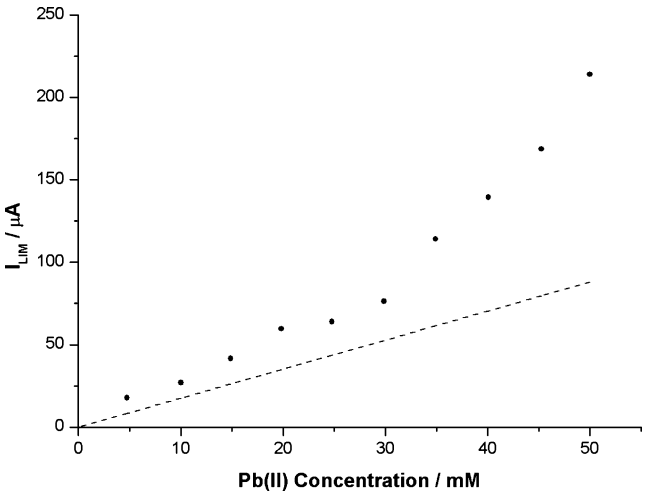

Fig. 9 Plot of I_{LIM} vs concentration for the reduction of Pb $(CH_3COO)_2.3H_2O$ at a glassy carbon RDE at 23 °C. Rotation rate=1,500 rpm, scan rate=0.005 V s^{-1}. Data points represented as *dots* are experimental values, whilst those designated by *dashes* provide the theoretical Levich straight-line plot (calculated using D=1.8×10^{-7} cm^2 s^{-1})

The relatively low D value obtained for Pb(II) in DIMCARB can be partly attributed to the high viscosity of this medium. In water, the D value for Pb^{2+} in 0.1 M KNO_3 is in the range of 79–83×10^{-7} cm^2 s^{-1} [31, 32]. The D value of 1.8×10^{-7} cm^2 s^{-1} calculated using the Compton–Hyde and de Vries–van Dalen approaches is consistent with the increase in viscosity of DIMCARB compared to water (DIMCARB has a viscosity ca. 80 times greater than water at 22 °C [10]).

Conclusions

The electrochemical reduction of Pb(II) in the 'distillable' ionic liquid, DIMCARB, has been studied. The results show that Pb(II) is reduced in a single two-electron step in this medium. The voltammetry results show that this reduction process occurs by a diffusion-controlled mechanism. Cyclic voltammetric and chronoamperometric data suggest that the Pb(II) reduction to the zerovalent state predominantly occurs via a 3-D diffusion, nucleation and growth mechanism. Analysis of the chronoamperometric data using the Hills–Scharifker theory indicates that the mechanism is progressive nucleation, and this conclusion is supported by SEM images that show nuclei of varying sizes on the electrode surface. Bulk electrolysis experiments suggest that elemental Pb is the deposited species. However, ex situ powder X-ray diffraction data show that α- and β-PbO_2 phases were also present. This oxide formation is tentatively attributed to the reaction of small particles of activated Pb with oxygen. Reduction of Pb(II) at a Hg thin-film electrode provide no evidence for a nucleation and growth reduction mechanism; instead, the reversible formation of a Pb–Hg amalgam is observed. The diffusion coefficient of Pb(II) in DIMCARB has been calculated to be 1.8±0.4×10^{-7} cm^2 s^{-1} by both the de Vries–van Dalen and Compton–Hyde approach, which is similar to the value predicted by the Hills–Scharifker nucleation and growth theory.

Acknowledgements The authors express appreciation to the Australian Research Council Special Research Centre for Green Chemistry for financial support. We would also like to gratefully acknowledge Mr. R. Pan and Dr. J. Etheridge for providing the SEM images, Mr. R. Mackie for assistance with powder X-ray diffraction measurements and the Royal Society for the award of a fellowship to A.I. Bhatt.

References

1. Welton T (1999) Chem Rev 99:2071
2. Wasserchied P, Kiem W (2000) Angew Chem Int Ed Engl 39:3772
3. Blanchard A, Hancu D, Beckman EJ, Brenecke JF (1999) Nature 399:28
4. Wasserchied P, Welton T (eds) (2003) Ionic liquids in synthesis. Wiley-VCH, Weinheim
5. Buzzeo MC, Evans RG, Compton RG (2004) ChemPhysChem 5:1106
6. Endres F (2002) ChemPhysChem 13:144
7. Zhang J, Bond AM (2005) Analyst 130:1132
8. Kreher UP, Rosamilia AE, Raston CL, Scott JL, Strauss CR (2004) Molecules 9:387
9. Kreher UP, Rosamilia AE, Raston CL, Scott JL, Strauss CR (2003) Org Lett 5:3107
10. Bhatt AI, Bond AM, Zhang J, MacFarlane DR, Scott JL, Strauss CR, Iotov PI, Kalcheva SV, Shaw R (2006) Green Chem 8:161
11. Katayama Y (2005) In: Ohno H (ed) Electrochemical aspects of ionic liquids. Wiley-VCH, Weinheim
12. Lin LG, Wang Y, Yan JW, Yuan YZ, Xiang J, Mao BW (2003) Electrochem Commun 5:995
13. Bard AJ, Faulkner LR (2001) Electrochemical methods: fundamentals and applications. Wiley, New York
14. Petersson I, Ahlberg E (2000) J Electroanal Chem 485:166
15. Palmisano E, Desimoni L, Sabbatini G, Torsi J (1979) J Appl Electrochem 9:517
16. Kelber J, Rudenja S, Bjelkevig C (2006) Electrochim Acta 51:3086
17. Ziegler JC, Wielgosz RI, Kolb DM (1999) Electrochim Acta 45:827
18. Yang M, Hu Z (2005) J Electroanal Chem 583:46
19. Mostany J, Mozota J, Scharifker BR (1984) J Electroanal Chem 177:25
20. Bulhões LOS, Mascaro LH (2004) J Solid State Electrochem 8:238
21. Scharifker B, Hills G (1983) Electrochim Acta 28:879
22. Hussey CL, Xu X (1991) J Electrochem Soc 138:1886
23. Skidmore PR, Schwarz RR (1979) Analyst 104:952
24. Bone SJ, Singh KP, Wynne-Jones WFK (1961) Electrochim Acta 4:288

25. Barradas RG, Hettgen IG, Girgis M (1988) J Electroanal Chem 243:435
26. Serruya A, Mostany J, Scharifker BR (1999) J Electroanal Chem 464:39
27. Sahlin E, Jagner D, Ratana-ohpas R (1997) Anal Chim Acta 346:157
28. Hyde ME, Compton RG (2005) J Electroanal Chem 581:224
29. de Vries WT, van Dalen E (1967) J Electroanal Chem 14:315
30. Stojek Z, Kublik Z (1997) J Electroanal Chem 77:205
31. Silva SM, Bond AM (2003) Anal Chim Acta 500:307
32. Heyrovsky J, Kuta J (1966) Principles of polarography. Academic, New York